Enhancement of x-ray line emission from plasmas produced by short high-intensity laser double pulses

A. A. Andreev
Institute for Laser Physics, S.C. Vavilov State Optical Institute, Birzhevaya line 12, 193232 St. Petersburg, Russia

J. Limpouch* and A. B. Iskakov†
Faculty of Nuclear Science and Physical Engineering, Czech Technical University in Prague, Břehová 7, 115 19 Prague, Czech Republic

H. Nakano
NTT Basic Research Laboratories, 3-1, Morinasato Wakamiya, Atsugi-Shi, Kanagawa 243-0198, Japan
(Received 9 October 2000; revised manuscript received 14 June 2001; published 23 January 2002)

Femtosecond laser-produced plasmas are bright ultrafast line x-ray sources potentially suitable for different applications including material science and biology. The conversion efficiency of the laser energy incident onto a solid target into the x-ray emission is significantly enhanced when a laser prepulse precedes the main pulse. The details of x-ray line emission from solid targets irradiated by a pair of ultrashort laser pulses are investigated both theoretically and experimentally. Insight into spatial and temporal characteristics of the line x-ray source is provided by numerical simulations and a simplified analytical model. Optimal time separation of the laser pulses is searched for in order to reach the maximum conversion of laser energy into the emission of selected x-ray lines. We deduced how the optimal pulse separation scales with laser and target parameters.

DOI: 10.1103/PhysRevE.65.026403 PACS number(s): 52.50.Jm, 52.25.Os, 52.65.−y

I. INTRODUCTION

The advanced technology of short pulse lasers now provides the opportunity to build sufficiently compact lasers with moderate and high repetition rates. The laser pulses can be focused to reach high intensities on a solid target and thus high-temperature, high-density plasma is produced. A certain part of the absorbed laser energy is converted into x-ray radiation that might be suitable for various applications, including material science. In particular, using such laser pulses, x-ray pulses with high power and short pulse duration may be achieved. Such x rays, synchronized by the incident laser pulse, are extremely important as diagnostic probes in the pump-probe-type experiments for observing the dynamic responses of optically excited materials. The laboratory x-ray sources discussed here also offer some specific advantages in comparison with the conventional x-ray sources, e.g., synchrotrons, such as compactness, easy access, relatively low cost, short pulse length, and small x-ray source size. The efficiency of such sources is, in general, quite high, but it is possible to further increase the x-ray yields for applications using a laser prepulse with suitable parameters.

An amplified spontaneous emission prepulse was previously found [1] to enhance or reduce the x-ray yield depending on experimental conditions. The enhancement of x-ray yield by short laser prepulses has been reported in several experimental papers [2–5]. However, no detailed theoretical description has been presented and optimization has not been attempted. The control and optimization of the x-ray emission from high-intensity laser-produced plasmas is a subject of current interest [6–8] and requires an understanding of laser absorption, thermal transport, and x-ray conversion processes. Significant enhancement of the x-ray source performance may be achieved by a careful choice of laser wavelength, pulse duration, intensity, and target material. Using suitable laser and target parameters, the laser plasma x-ray source may reach a peak brilliance comparable to a large synchrotron facilities [9]. This reference demonstrates the possibility of enhancing line x-ray emission by optimization of foil target parameters. However, using laser prepulse is simpler from the experimental point of view and high repetition rates may be achieved more easily.

The choice of parameters depends crucially on a particular application of the x-ray source. Aluminum targets seem to be suitable for pulse-probe diagnostics of semiconductor surfaces [10], targets including lithium are promising for microlithography [11], while carbon targets may be used in biology. The possibilities of source optimization of high power picosecond x-ray pulses in ''water window'' were studied in [12]. For certain applications short laser wavelengths may be beneficial, as laser energy is deposited at higher plasma densities and weaker nonlinear effects in laser-target interaction make it easier to control target heating. However, a high repetition rate of the x-ray source is essential for many applications and this is achieved by means of Ti:sapphire laser or its second harmonics.

In this paper, the possibility of x-ray source optimization using subpicosecond laser pulses with a suitable laser prepulse is studied both theoretically and experimentally. Recent developments in x-ray optics instrumentation [5] make Ly-α and He-α emission particularly interesting. We shall concentrate here on the He-α line, since it is the most intense resonance line for the intensities considered. Laser radiation incident normally on the target is assumed here, although the

*Author to whom correspondence should be sent; email address: limpouch@lilit.fjfi.cvut.cz

†Permanent address: Institute of Mathematical Modeling, Miusskaya sq. 4a, 125047 Moscow, Russia.

efficiency of laser energy transformation into x-ray emission is generally higher for *p*-polarized radiation incident at an optimum angle. However, problems caused by fast electrons are avoided using normal incidence and the control of laser-plasma interaction is improved. The loss in the energy transformation efficiency is relatively small when a suitable laser prepulse is used. Recent experimental results [13] indicate that by using a normally incident laser beam preceded by a suitable prepulse, the energy transformation efficiency into line x-ray emission may be significantly higher than for a *p*-polarized laser pulse incident without a prepulse at an optimum angle (no additional optimization is assumed).

Our paper presents the results of both theoretical and experimental investigations into the enhancement of x-ray energy emitted from aluminum plasma created by a pair of femtosecond laser pulses. Time-integrated x-ray spectra were measured for various time intervals separating the prepulse and the main pulse. The amount of x-ray emission in lines was greatly enhanced at an optimum temporal pulse separation. One- and two-dimensional (2D) hydrodynamics computer codes are applied for the numerical simulation of the laser pulse absorption and of the plasma dynamics. They are coupled to a post-processor code for a detailed calculation of the radiation transport in x-ray lines. The computer simulations also reveal the temporal and spatial characteristics of the line x-ray source that are difficult to obtain directly from the experiment.

II. EXPERIMENT SETUP

The experiments were performed with a Ti:sapphire laser system operating at 10 Hz at a wavelength of $\lambda_L = 790$ nm. It provided laser pulses of energy $E_L = 30$ mJ, and full width at half maximum (FWHM) pulse duration $\tau_L = 100$ fs. Using a Mach-Zehnder-type interferometer, the laser pulse was split into two parts to form a prepulse and a main pulse with a variable time delay ($0 \leqslant \Delta\tau \leqslant 3$ ns). Both pulses were focused on the target at normal incidence with a 200-mm focal length MgF_2 lens, laser beam diameter of focusing lens was 30 mm. The focal spot diameter was about 30 μm, and the peak intensity was 2.3×10^{16} W/cm^2 (for details see [4,14]). The extinction ratio between the main pulse and undesirable satellite pulses that preceded by more than 1 ns was better than 10^6 on the target so that preplasma formation was avoided. As a target, 4-μm-thick aluminum film deposited on a silicon wafer was used. A spherically bent mica crystal ($2d = 1.994$ nm) with a bend radius of 100 mm was used to measure x-ray emission spectra in the keV range. Using an independent ultrashort laser pulse at smaller intensity as a prepulse makes it easy to adjust the parameters of preformed plasma. Time-integrated x-ray spectra were measured for varying time intervals separating the prepulse and the main pulse. At relatively large time separations the amount of x-ray emission was greatly enhanced [15] (see Fig. 5).

III. SIMULATION MODEL

The main motivation for our study is the conversion of laser energy into a very narrow region of x-ray spectra, e.g., into a single spectral line or a group of neighboring lines. When an intense laser beam interacts with a low or medium Z target, the energy emitted in lines is relatively small (less than a few percent). Thus, detailed atomic physics and line emission may be solved using a post-processor to the code simulating laser-plasma interaction. Here normally incident short laser pulses of moderate intensities ($\lesssim 10^{16}$ W/cm^2) are considered, and the interaction is tractable using hydrodynamics models.

One-dimensional planar geometry is usually a good approximation for the interaction of subpicosecond laser pulses with solid targets, the plasma expansion being much smaller than the laser spot diameter. Some one-dimensional hydrodynamics codes [16,17] have been tailored in order to provide a reasonably accurate description of short pulse target interactions for low and moderate laser intensities. However, in this paper we also model a different situation, when the main pulse delay is so large that the expansion length of plasma formed by the prepulse is much greater than the laser spot diameter. Thus, a combination of one- and two-dimensional hydrodynamics codes is applied here. The primary aim of the 2D simulations is to find the profile of plasma parameters on the laser beam axis at the rise of the main laser pulse. The two-dimensional model is also used to show that the interaction of the main laser pulse with the target and the line x-ray emission from plasma may be treated in 1D geometry with reasonable accuracy.

Both 1D and 2D hydrodynamics codes used here are one-fluid two-temperature Lagrangian codes. The hydrodynamics code used for a one-dimensional description of the laser-plasma interaction and of the plasma dynamics is described in detail in Ref. [16]. Laser absorption is calculated by numerical solution of Maxwell's equations for both *s*- and *p*-polarized laser radiation. A simplified model of atomic physics is included in the hydrodynamics model in order to calculate the average ion charge Z and the averaged ion charge squared $\overline{Z^2}$. The populations of the ion charge states are calculated from the set of atomic rate equations. The rates of collisional ionization, radiative, and three-body recombination, taken from the paper [18], include the depression of the ionization potential in dense plasmas.

The laser radiation is incident normally on the target in the present experiments and it is absorbed mainly collisionally. Thus, a detailed model of complex dielectric constants in dense plasma is essential for an accurate calculation of absorption efficiency; the model proposed in Ref. [19] is applied here. Laser absorption is calculated by solving Maxwell's equations on fine spatial grid; no additional energy damping at the critical surface is added. Due to the large f number $f/7$ of the focusing optics, resonance absorption is rather small. One expects an increase in absorption due to nonlinear collisionless absorption, but it is hard to estimate for normal incidence and a certain part of the absorbed energy is transported deep into the target by fast electrons with minimum influence on the corona dynamics and on resonance line emission.

The theory described in [20] is used for the rate of tunneling ionization by laser radiation. However, the density of free electrons in solid aluminum is high and the critical sur-

face coincides with the target surface before laser pulse arrival. Thus, tunneling ionization is not as important here as it is for dielectrics. The maximum laser intensities here are substantially below the threshold for ionization to ion charge $Z=5$.

The two-dimensional hydrodynamics simulations are conducted with the cylindrical version of the code ATLANT [21]. This is a Lagrangian code with natural and artificial viscosity, electron and ion heat conductivity. The heat flux limitation is included via flux limiter *f*. Plasma atomic physics is described here via average atom approximation. A ray-tracing algorithm is used for laser propagation; collisional laser absorption in underdense plasma is included. However, the spatial resolution is insufficient to calculate the laser reflection near the critical surface in detail; therefore, a specified portion of laser energy is dumped in the hydrodynamics cell, where the laser reflection occurs. The overall absorption efficiency of the prepulse and of the main pulse is taken from the one-dimensional model.

When plasma line x-ray emission is calculated, the assumption of the local thermodynamic equilibrium cannot be used, due to both the insufficient thickness and the fast transient nature of the source. On the other hand, the impact of the reabsorption of the emitted line radiation on the ionic populations has to be taken into account, at least for the most intense resonance lines. Previously [22], selected methods from astrophysics were modified for model studies of homogeneous and static laboratory plasmas. For laboratory plasmas a model of radiation transfer based on escape factors was developed in Ref. [23]. However, the macroscopic Doppler shift was not taken into account when the escape factors were derived and this was the main drawback of this approach. Alternatively, Sobolev escape factors were used for modeling [24] of x-ray emission from a short-pulse laser-produced plasma. These escape factors take into account the macroscopic Doppler shift; however, only Doppler broadening is included. A ''localized'' Newton-Raphson method, proposed in [25], has the capability to include a macroscopic Doppler shift simultaneously with the general line profile. When the rate equations are solved, the spectral intensity dependence on populations is limited to one Lagrangian cell in each iteration step of the rate equations and then radiative transfer through the entire grid is evaluated after each iteration step. We have adopted this method, and a reasonably fast convergence of this scheme has been confirmed.

Radiation transport in x-ray lines is solved here in 1D planar geometry. The plasma parameters (density, velocity, electron and ion temperature) are taken from the hydrocode output, where they are represented in a grid of Lagrangian cells. The radiative field is calculated only for the selected bound-bound transitions, which can be optically thick and can influence the populations significantly. The spectral radiation intensity for these lines is characterized in a frequency grid. The 1D radiation transfer equation is solved in the planar geometry,

$$\frac{1}{c}\frac{\partial I_\nu}{\partial t}+\mu\frac{\partial I_\nu}{\partial x}=j_\nu-k_\nu I_\nu, \tag{1}$$

where $\mu=\cos\theta$, θ is the propagation angle of radiation with respect to the target normal, j_ν and k_ν are the spectral emission and the absorption coefficients, respectively. As the transit time of radiation through plasma is negligible, radiative transfer is solved in the approximation of the infinite speed of light, i.e., neglecting the first term of the above equation.

The atomic physics model is designed for *K*-shell spectroscopy and it includes a detailed system of resonance levels for Li-, He-, and H-like states, as well as several dielectronic states important for x-ray diagnostics, so that the emission of satellite lines to Ly-α and He-α lines may be calculated. The number of states included is limited by the lowering of the ionization potential in dense plasma or for lower densities by the atomic physics database. The database is implemented for aluminum and carbon ions, and includes all the collisional and radiation processes, but in the present version it assumes Maxwellian electron distribution. The rate equation governing the population of the level *k* is written, as follows:

$$\begin{aligned}\frac{\partial N_k}{\partial t}=&\sum_l\left[-N_kA_{kl}+(B_{lk}N_l-B_{kl}N_k)\frac{4\pi}{c}\overline{J}_{kl}\right]\\&-\sum_n C_{kn}(n_e,T_e)N_k+\sum_m\left[N_mA_{mk}-(B_{km}N_k\right.\\&\left.-B_{mk}N_m)\frac{4\pi}{c}\overline{J}_{mk}\right]+\sum_n C_{nk}(n_e,T_e)N_n,\end{aligned} \tag{2}$$

where N_k is the population density of the level *k* and A_{kl}, B_{lk}, and B_{kl} are Einstein coefficients of spontaneous emission, absorption, and stimulated emission, respectively. The first term represents radiative bound-bound transitions between the level *k* and the lower level *l*, while the third term stands for radiative bound-bound transitions between the level *k* and upper level *m*. The sum of all possible collisional transitions from and to level *k* is described by the second and fourth terms. The collisional rate coefficients C_{nk} depend generally on electron density n_e and temperature T_e and include collisional excitation and deexcitation, collisional ionization, radiative and three-body recombination, autoionization, and dielectronic recombination. Photoionization is not included, as plasma is assumed to be optically thin for continuum radiation. The absorption and the stimulated emission of the spectral lines are the only nonlinear terms in the rate equations. Their nonlinearity arises from the dependence of the mean integrated intensity $\overline{J}_{kl}$,

$$\overline{J}_{kl}=\tfrac{1}{2}\int_{-1}^{1}d\mu\int_0^\infty I_\nu(x,\mu)\Phi_\nu^{kl}(x,\mu)d\nu, \tag{3}$$

on the population densities. The integration is performed over angle and frequency, and identical emission and absorption line shape Φ_ν^{kl} is assumed.

The coefficient of spontaneous emission j_ν and the coefficient k_ν of absorption and stimulated emission for transition between an upper level *k* and a lower level *l* are specified by the following expressions:

$$j_\nu^{kl}(x,\mu)=\frac{h\nu_{kl}}{4\pi}A_{kl}N_k(x)\Phi_\nu^{kl}(x,\mu), \tag{4}$$

$$k_\nu^{kl}(x,\mu)=\frac{c^2}{8\pi\nu_{kl}^2}\frac{g_k}{g_l}\left(N_l(x)-\frac{g_l}{g_k}N_k(x)\right)\Phi_\nu^{kl}(x,\mu),$$

where ν_{kl} is the frequency of the kl transition and g_k is the degeneracy of the level k.

In the implemented model, the nonequilibrium line transfer is computed within the core saturation approximation [26]. This approach is used both for the acceleration of the convergence and for better description of the variation of the radiative intensity within each hydrodynamic cell. We assume a Voigt profile of emission and absorption line

$$\Phi_\nu^{kl}(x,\mu)$$

$$=\frac{\Gamma^{kl}(x)}{4\pi^{5/2}\ln 2}\int_{-\infty}^{\infty}\frac{\exp(-y^2)dy}{\frac{\Gamma^{kl}(x)^2}{16\pi^2}+\left[\nu-\nu_{kl}(x,\mu)-\frac{\nu_D^{kl}(x)}{2\sqrt{\ln 2}}y\right]^2}, \tag{5}$$

where ν_D is the Doppler width, while Γ is the Lorentz width, taking into account natural, lifetime, and electron impact Stark broadening. A macroscopic Doppler shift due to the plasma velocity is included in the frequency $\nu_{kl}(x,\mu)$ of the transition, which depends explicitly on the coordinate and the propagation direction of radiation in the laboratory frame. Quasistatic Stark broadening due to ion microfields is incorporated in a rather crude approximation, using Holtzmark microfield distribution [27]. Only efficient line broadening is included, as a more general form of line profile is needed for a precise description of ion Stark broadening. This is a serious drawback, especially for line shape measurements. However, the exact shape of the emission line may not be crucially important here for the energy emitted (observation angle 45°), as the line reabsorption is substantially reduced due to the macroscopic Doppler shift in the expanding plasma. Moreover, we shall concentrate mainly on He-α line emission, and the impact of ion microfields is much less important for this line than it is for the emission of H-like ions. The generalization of the line profile is planned to be incorporated into the code in the near future. The equations for radiative transfer are solved together with the level populations only for potentially optically thick lines.

1D planar geometry is assumed in the post-processor, even when a laser prepulse is present. This assumption is substantiated by 2D hydrodynamics simulations showing that only a relatively thin layer (typically 10–20 μm for 2 ns delay) behind the critical surface is ionized up to the He-like state and this region is responsible for most of the K-shell line emission. During the x-ray emission this layer is placed typically only 0–30 μm away from the original target surface for 2 ns delay. This is comparable to the size of the focal radius, and thus the plasma expansion is very close to planar here. The importance of deviations from the planar expansion far from the target is further reduced since the bulk Doppler shift due to plasma motion suppresses the reabsorption of spectral lines.

As stated above, the post-processor code calculates atomic level populations taking into account the impact of the radiation transfer in selected x-ray lines. Then, using the populations obtained, the spectra emitted in any direction are determined. The fluence F^{kl}, which may be compared to the energy emitted in the experiment divided by the focal spot surface, is given by the integration over frequency and time

$$F^{kl}(\mu)=\int dt\int_{\nu_{kl}} I_\nu(x_b,\mu)d\nu, \tag{6}$$

where x_b is the plasma vacuum boundary and the integration over frequency is restricted to the given line.

IV. ANALYTICAL MODEL

We have developed an approximate analytical model of laser-target interaction and He-like resonance line emission. This model reveals basic qualitative scaling relations of the emitted energy on prepulse and main pulse parameters. This model was introduced in our earlier work [15]. However, it was explained very briefly there and it contained some misprints. The model estimates the dependence of the fluence emitted in He-α resonance line on laser and target parameters.

Simple models are used for the description of the principal processes during the interaction of the prepulse and of the main pulse with target. Laser prepulse heats a part of the target, producing dense plasma of electron density n_{e0} and ion sound velocity $c_{s0}=\sqrt{Z_0T_{c0}/A_mM_p}$. The characteristic dimension of the heated region is $L_0=c_{s0}\tau_p$, where τ_p is the prepulse duration. We shall develop our model using the above quantities and we shall postpone the detailed description of the prepulse interaction to the end of this section.

The expanding plasma cools down during the gap $\Delta\tau$ between the prepulse, and the main pulse. After the laser prepulse, the electron temperature decreases with time t according to the relation $T_e\simeq T_{e0}\tau_p/t$. Plasma scale length at the main pulse rise (i.e., at the end of the gap $\Delta\tau$) is expressed as

$$L=c_{s0}\left(\frac{\tau_p}{\Delta\tau}\right)^{1/2}\Delta\tau=c_{s0}\sqrt{\tau_p\Delta\tau}=L_0\left(\frac{\Delta\tau}{\tau_p}\right)^{1/2}.$$

Plasma electron density n_e at the main pulse rise depends on the geometry of plasma expansion during the gap $\Delta\tau$ between the prepulse and the main pulse,

$$n_e=n_{e0}\left(\frac{L_0}{L}\right)^\chi=n_{e0}\left(\frac{\tau_p}{\Delta\tau}\right)^{\chi/2},$$

where $\chi=1,2,3$ for planar, cylindrical, and spherical expansion geometry, respectively.

The electron temperature T_e of plasma heated by the main pulse is found from the energy conservation

$$n_eLT_e=A_LF_L,$$

where F_L is the main pulse fluence and A_L is the main pulse absorption efficiency. The density scale length L during the main pulse is much larger than laser wavelength, and thus the absorption efficiency scales $A_L \sim ZLT_e^{-3/2}$ and the average ion charge is $Z \sim T_e^{1/3}$ [28]. We assume that this scaling leads to the absorption $A_L < 1$ and the electron temperature is found as

$$T_e = C_T \left(\frac{\Delta\tau}{\tau_p} \right)^{6\chi/13} \left(\frac{F_L}{n_{e0}} \right)^{6/13}, \tag{7}$$

where C_T is a multiplicative constant depending on the laser wavelength and on the target material.

When the electron density and temperature is known, atomic physics may be solved. The target ions are gradually ionized up to the He-like state during the duration τ_L of the main pulse. It is assumed that most of the time is spent on collisional ionization from the Li-like to the He-like state. Thus, the concentration of He-like ions created by collisional ionization of Li-like ions during the main pulse can be written as

$$N_{\mathrm{He}} = C_l n_e^2 T_e^{1/2} \exp(-J_{Li}/T_e)\tau_L,$$

where J_{Li} is the ionization potential of Li-like ions and C_l is a constant depending on the target material. As the ionization potential of the He-like ion is much larger than that of the Li-like ion, ionization of He-like ions may be considerably slower if the target temperature is not too high. Also, the excitation energy of the He-like ion is much higher than J_{Li}, and thus nearly all ions ionized to the He-like stage stay in the ground state. The concentration N_1 of the He-like ions in the ground state is thus $N_1 \simeq N_{\mathrm{He}}$. The equilibrium population of the first excited He-like state $1s2p:{}^1P$ state is

$$N_2 = N_1 \frac{g_2}{g_1} \exp(-E_{21}/T_e) = N_{\mathrm{He}} \frac{g_2}{g_1} \exp(-E_{21}/T_e),$$

where $g_1 = 1$ and $g_2 = 3$ are statistical weights of the respective states, E_{21} is the energy difference of the respective states.

Optically thin plasma is assumed and the emitted fluence is

$$F_X = N_2 A_{21} E_{21} L \tau_{\mathrm{em}},$$

where A_{21} is the Einstein coefficient of spontaneous emission and τ_{em} is the emission time. The characteristic time of resonance photodeexcitation is $A_{21}^{-1} \simeq 36$ fs for aluminum. Thus, fast decay of resonance emission during plasma cooling after the main pulse is assumed and the emission time is approximated by the main pulse duration $\tau_{\mathrm{em}} \simeq \tau_L$. After the substitution for N_2 and L, the fluence F_X of He-α emission may be expressed as

$$F_X = A_{21} E_{21} C_T^{1/2} C_l \frac{g_2}{g_1} c_{s0} \tau_p \tau_L^{29/13} I_L^{3/13} \left(\frac{\tau_p}{\Delta\tau} \right)^{(23\chi-13)/26} \times \exp\left[-\frac{E_{21}+J_{Li}}{C_T} \left(\frac{n_{e0}}{I_L \tau_L} \right)^{6/13} \left(\frac{\tau_p}{\Delta\tau} \right)^{3\chi/13} \right], \tag{8}$$

where $I_L = F_L/\tau_L$ is the main pulse intensity.

There exists an optimum delay $\Delta\tau_m$ of the main pulse when He-α emission is maximum. If we denote $x = \Delta\tau_m/\Delta\tau$, then the emitted fluence is

$$F_X = F_m x^{(23\chi-13)/26} \exp[-\beta(x^{3x/13}-1)], \tag{9}$$

where $\beta = (23\chi-13)/6\chi$ depends on the geometry of plasma expansion. The optimum main pulse delay is

$$\Delta\tau_m = \tau_p \tau_L^{-2/\chi} \left(\frac{n_{e0}}{I_L} \right)^{2/\chi} \left[\frac{E_{21}+J_{Li}}{C_T \beta} \right]^{13/3\chi}. \tag{10}$$

Experimentally, the easiest way is to make a prepulse of the same length as the main pulse $\tau_p = \tau_L$ and then for $\chi = 2$ the optimum delay $\Delta\tau_m$ does not explicitly depend on laser pulse lengths and it decreases with the increasing laser intensity I_L.

The maximum emitted fluence F_m and the optimum pulse delay $\Delta\tau_m$ may be explicitly expressed when the interaction of the prepulse with the target is specified in detail. The electron density n_{e0} of the prepulse plasma is estimated $n_{e0} = Z_0 \rho_0/(A_m M_p)$, where M_p is the atomic mass unit, A_m is the target mass number, and ρ_0 is the cold target density. The average ion charge Z_0 of the prepulse plasma grows with the plasma electron temperature T_{e0}. This is found from the prepulse absorption as follows:

$$T_{e0} = \frac{A_m M_p}{Z_0} \left(\frac{A_p I_p}{\rho_0} \right)^{2/3},$$

where I_p is the prepulse intensity. The prepulse absorption A_p can be expressed for the density scale length L_0 in the interval $0.01 < L_0/\lambda < 0.1$ by the scaling formula [30]

$$A_p = 0.2 \left(\frac{\nu_c}{\omega_0} \right)^{0.7} \left(\frac{\lambda}{L_0} \right)^{0.3} \left(\frac{n_{e0}}{n_c} \right)^{0.2},$$

where ν_c is the electron-ion collision frequency at the critical surface, ω_0 and λ are the laser frequency and wavelength, and n_c is the critical density. The multiplicative constant C_T is the only free parameter of the analytical model that can be varied to a certain extent to match the model results with the experiment.

V. SIMULATION RESULTS AND COMPARISON WITH EXPERIMENT

In the present experiments, the laser radiation is incident normally on the target. Without a laser prepulse the absorption efficiency of a short intense pulse incident normally onto a perfect solid target is generally rather low, about 15% [29]. The prepulse forms plasma that is expanding and cooling down before the main pulse arrives. The absorption of the normally incident laser beam depends on the extent and density of plasma already present. The absorption efficiency of the normally incident main pulse versus the time separation between the prepulse and the main pulse for the conditions of the present experiment is displayed in Fig. 1.

It is shown that for rather short pulse separations,

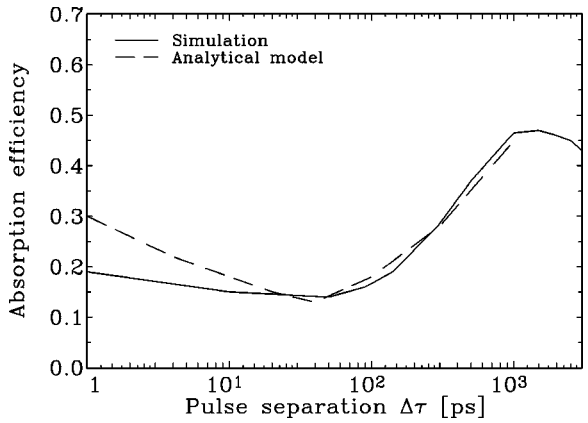

FIG. 1. Absorption efficiency of the main laser pulse incident normally onto a solid Al target vs the pulse separation $\Delta\tau$. Gaussian laser pulses of FWHM length $\tau_L=100$ fs and wavelength $\lambda_L=790$ nm are assumed. The main pulse intensity is $I_L=2.3\times10^{16}$ W/cm^2, while the prepulse intensity is $I_p=10^{15}$ W/cm^2.

$\Delta\tau\lesssim100$ ps, the absorption efficiency is even lower than in the case when no prepulse is present. A layer of expanding plasma inhibits laser penetration into dense plasma by the skin effect and the absorption of the normally incident wave is thus reduced [4,30]. The absorption efficiency rises significantly for longer pulse separations, as collisional absorption is efficient in a plasma region with large density scale length formed by the prepulse. The calculated absorption efficiency is compared with our analytical formula, deduced in paper [30] for exponential density profile, and a good agreement between analytical and simulation results is demonstrated in Fig. 1. For pulse separations longer than 1 ns, the density of plasma formed by the prepulse declines, and, therefore, the absorption efficiency gradually decreases.

We note that velocity $v_{\rm osc}=e\mathcal{E}_L/m_c\omega_0$ of electron oscillation in laser electric field $\mathcal{E}_L$ at the main pulse maximum is comparable to the electron thermal velocity $v_e=(k_BT_e/m_e)^{1/2}$ and the maximum values of Langdon [31] parameter $\alpha=Zv_{\rm osc}^2/v_e^2$ up to 5 are reached. An upper estimate of the decrease in collisional absorption due to the deviations from Maxwellian velocity distribution is obtained when in each spatial-temporal point electron distribution is assumed to be equal to the time-asymptotic electron distribution for local and instant value of parameter α. Then the decrease in electron-ion collision frequency is calculated according to the fitting formula derived in [31]. The computed upper estimates of the decrease in the overall efficiency of the collisional absorption are $\lesssim$20% for the conditions of experiments [4] and all assumed pulse separations. On the other hand one expects an increase in absorption due to collisionless effects [29].

When the pulse separation is short, $\Delta\tau\lesssim100$ ps, *p*-polarized obliquely incident radiation is absorbed much more efficiently, leading to a much higher energy conversion to x-ray emission. For large density scale lengths, corresponding to pulse separations $\Delta\tau\gtrsim500$ ps, there is almost no difference between absorption efficiency for *s*- and *p*-polarized obliquely incident radiation [13]. Thus, it might be more suitable to use a normally incident laser pulse for our purposes because generation of fast electrons is minimized for normal incidence and the control of experiments is improved.

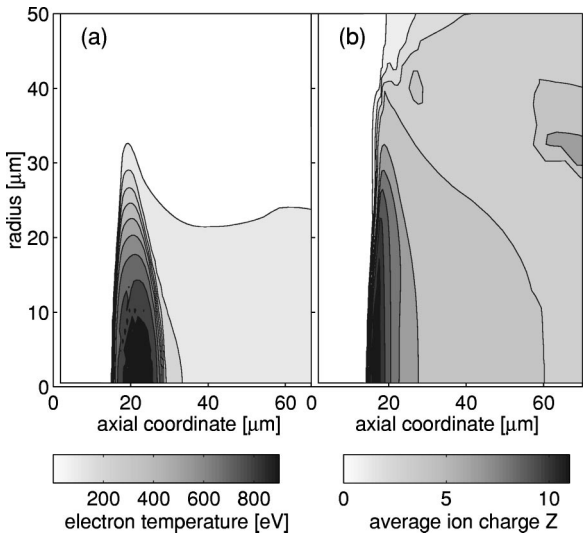

FIG. 2. Electron temperature (a) and ion average charge (b) spatial distributions near the target surface 2 ps after the main laser pulse maximum. The main laser pulse of intensity $I_L=2.3\times10^{16}$ W/cm^2, $\tau=100$ fs, and $\lambda_L=790$ nm is incident from the right onto a solid Al target with the delay $\Delta\tau=2$ ns after 100 fs prepulse of intensity $I_p=10^{15}$ W/cm^2. The laser beam FWHM radius on the target is 15 μm, the axial coordinate of the original target surface 15 μm.

For a significant delay, $\Delta\tau\gtrsim500$ ps between the prepulse and the main pulse, the results of two-dimensional hydrodynamics simulations show that the main pulse is absorbed in a relatively thin dense plasma layer near the surface of the target. Since the multiphoton ionization at laser intensities 10^{16} W/cm^2 is unable to ionize aluminum to the Li-like stage, the collisional ionization is dominant. It is efficient mostly in dense plasma, and thus the highest ionization is reached in overdense plasma behind the critical surface. The collisional ionization is highly nonstationary and nonequilibrium for 100 fs laser pulses. In our simulations, the highest intensity of the emission in He- and H-like lines is achieved approximately at 2 ps after the main pulse maximum. The spatial distributions of electron temperature and of the mean ion charge near the target surface are plotted at that moment in Fig. 2. The axial dimension of the overall plasma expansion is much larger, reaching up to 600 μm. Electron temperature on the axis has only one maximum near the original surface of the target. In addition to the primary maximum $Z\approx11$ at the axial coordinate ≈20 μm, there is a secondary maximum of the average ion charge $Z\approx7$ on the axis at a distance of approximately 200 μm from the target surface [not seen in Fig. 2(b)] in rarefied plasma. This corresponds to the remnants of the expanding plasma ionized by the laser prepulse. A part of these remnants may be seen in Fig. 2(b) at the radius $\simeq35$ μm and the axial coordinate >60 μm. However, the *K*-shell emission is generated exclusively in a narrow layer of hot, dense, and highly ionized plasma near the original target surface. The figure clearly depicts the planar

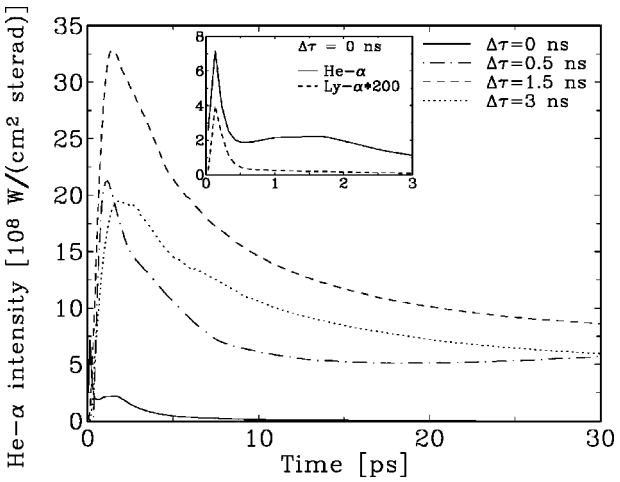

FIG. 3. Temporal intensity profiles of He-α emission in a direction 45° from the target normal for various time separations $\Delta\tau$ between the prepulse and the main pulse. Time $t=0$ corresponds to the main laser pulse maximum. In the inset Ly-α and He-α emission intensities are plotted, when no prepulse ($\Delta\tau=0$) is present. Identical experimental conditions as in Fig. 2.

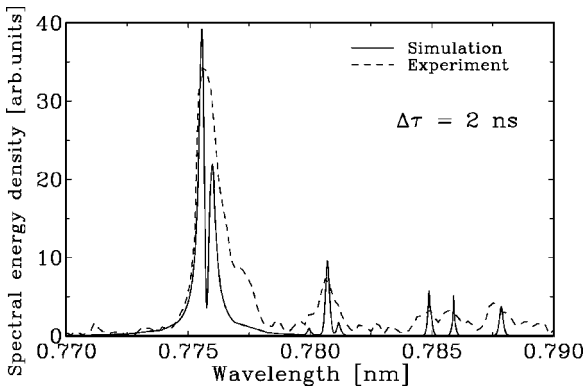

FIG. 4. Comparison of the calculated and experimentally measured x-ray spectra near He-α line, emitted in direction a 45° from the target normal. Time separation between the prepulse and the main pulse is $\Delta\tau=2$ ns. Identical experimental conditions as in Fig. 2.

geometry of this layer justifying the planar geometry used for post-processing of the hydrodynamics results, as already mentioned above.

Our simulations do not include self-generated magnetic fields that are often important in short-pulse laser-target interactions at high intensities [32]. Simple estimates, using exclusively $\nabla n_e \times \nabla T_e$ source term, show that magnetic field maximum $B \lesssim 100$ kG is reached at the focal spot edge. The electron cyclotron frequency for the maximum magnetic field is consideraby less than electron-ion collision frequency at the critical surface and thus magnetic-field-induced inhibition of thermal transport in negligible. Self-generated magnetic fields tend to reduce plasma expansion in the transverse direction at low densities but they have a much smaller impact on the plasma density profile in the focal spot center near the target surface.

One-dimensional hydrodynamics simulations are started at the rise of the main pulse using the profiles of plasma parameters, obtained in 2D simulations on the axis. The results of 1D hydrodynamics simulations are post-processed in order to obtain the populations of excitation states of Li-, He-, and H-like ions and *K*-shell emission spectra. The post-processor results also provide information about the experimentally unavailable temporal profile of x-ray emission. The length of the x-ray pulse may be a very important parameter for certain applications of line x-ray sources. The calculated temporal profiles of emitted He-α line intensities are plotted in Fig. 3. The inset displays the shapes of He-α and Ly-α pulses for the pulse separation $\Delta\tau=0$ ns. Generally, when no laser prepulse ($\Delta\tau=0$ ns) is present, the pulses of H-like resonance lines are subpicosecond; however, their integrated energy is rather small for intensities considered here. Pulses of He-like lines are generally longer; here a subpicosecond pulse of He-α emission is accompanied by an energetic tail approximately 3 ps long. When a laser prepulse is used, the energy conversion into line x-rays is considerably increased, however, the pulses of x-ray resonance lines become inevitably somewhat longer. Here, He-α emission pulse of $\approx$5 ps FWHM length is followed by a $\approx$30 ps long tail. The duration of x-ray line emission may be varied to a certain extent by variable laser pulse separation.

The x-ray spectrum emitted in a direction 45° from the target normal is measured in the experiment. The computed and experimental spectra in the neighborhood of the He-α line are plotted in Fig. 4 for the laser pulse separation $\Delta\tau=2$ ns. The ratios of resonance, intercombination, and satellite lines compare favorably. The widths of the satellite lines seem to be underestimated to a certain extent in the simulations, probably because a rather simple model of the line shapes is used in the post-processor. The figure demonstrates the ability of our approach to compute emission x-ray spectra for the assumed experimental conditions with reasonable accuracy.

One of the main goals of this work is to improve the laser energy transfer to He-α line emission by a laser prepulse. X-ray line emission increases with laser intensity, since it follows plasma temperature. However, when the plasma temperature is too high, the plasma may be ionized up to the H-like stage and the emission of He-like ions may be reduced. Another condition for the optimum x-ray line emission from a bulk target is the requirement that plasma should not be optically thick for the desired x-ray line, since the reabsorption reduces the amount of emission escaping from the plasma. The assumptions of the present model differ from those of Ref. [5], where a small pulse separation was assumed and thus the plasma corona average density was assumed higher than the critical density.

The enhancement of integrated line emission energy by the laser prepulse versus the laser pulse separation $\Delta\tau$ is shown in Fig. 5. Both the experiment and the simulations clearly demonstrate maximum energy of He-α line at the optimum pulse separation $\Delta\tau_m \approx 1.5-2$ ns. A satisfactory agreement between the experimental results and numerical simulations for He-α line emission is also apparent in the

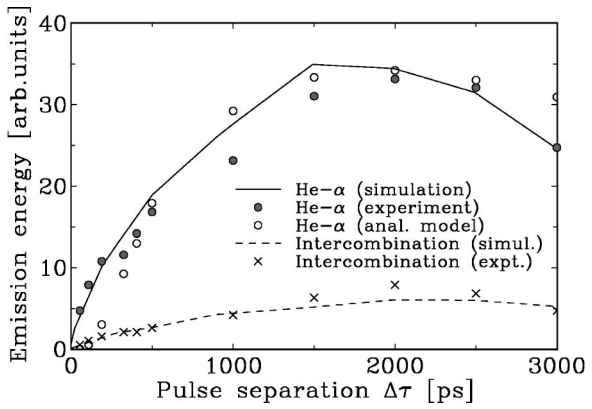

FIG. 5. The energy emitted in He-α and in the intercombination line vs the laser pulse separation $\Delta\tau$ in the present experiment. Identical experimental conditions as in Fig. 2. Analytical model data are plotted for $\chi=2$.

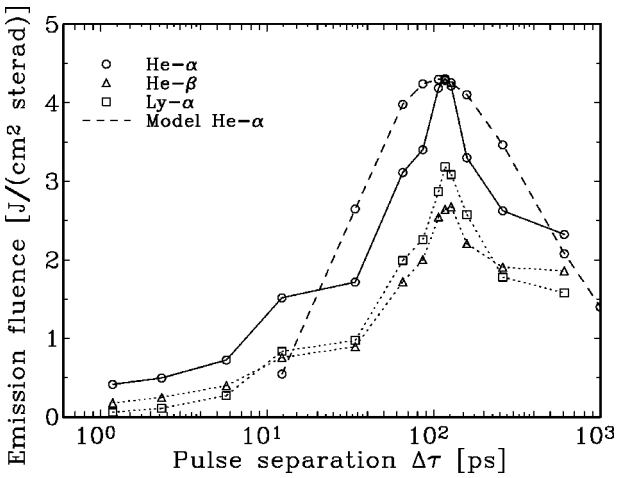

FIG. 6. The fluence emitted from an Al target in He-α, He-β, and Ly-α lines vs the pulse separation $\Delta\tau$, calculated for the following laser parameters: laser wavelength $\lambda_L=248$ nm, pulse length $\tau_L=600$ fs, main pulse intensity $I_L=5\times10^{16}$ W/cm^2, and prepulse intensity $I_p=3\times10^{15}$ W/cm^2. For the He-α line, the simulation results are compared to the analytical model ($\chi=2$).

shape of the curve. The expansion of prepulse-generated plasma is close to planar ($\chi=1$) for small pulse separation, while it is close to spherical ($\chi=3$) for large separation times, so no single value of χ is appropriate for all separation times. As a compromise, the results of the analytical model are plotted for $\chi=2$ in Fig. 5 and this choice of χ leads to a certain underestimation of resonance line emission for short-pulse separations. Due to the lack of absolute calibration in the experiment, arbitrary units are used in Fig. 5. The calculated maximum He-α emission energy (emission angle 45° to the target normal) is 0.034 J/cm^2/sterad. When this is multiplied by the solid angle 2π, laser energy transformation efficiency 5.9×10^{-5} into He-α emission is obtained.

The dependence of x-ray line emission energy on the pulse separation $\Delta\tau$, plotted in Fig. 5, demonstrates the possibility of substantial improvement in the efficiency of energy transformation into a particular x-ray line. For the relatively low laser intensity used in our experiment [4], the optimum pulse separations $\Delta\tau_m\approx1$ ns are much larger than in [5], where the optimum pulse separation of approximately 20 ps was determined for ≈1 ps laser pulses and the main pulse intensity $\simeq3\times10^{17}$ W/cm^2. This difference in the optimum pulse separation is reproduced well by our scaling, Eq. (9), which predicts an increase in the optimum pulse separation $\Delta\tau_m$ with decreasing energy of incident laser pulses.

In order to check the scaling of the optimum pulse separation with laser intensity and pulse length, we have performed our simulations for the conditions taken from [3]. In this experiment, the effect of a short prepulse (0.5 ps) on soft x-ray spectra from a plasma produced by a high-intensity KrF laser pulse of intensity $I_L=5.3\times10^{15}$ W/cm^2 and pulse length $\tau_m=0.5$ ps was studied. Both integrated emission in the spectral range 30–170 Å and the x-ray line emission of Li-like Al (transition $1s^23p$-$1s^22s$) are enhanced by laser prepulse and have a maximum at pulse separation $\Delta\tau\simeq150$ ps. Since here we are interested in emission of higher energy photons, approximately ten times higher laser intensity is assumed. The integrated energies of x-ray line emissions from plasma are plotted in Fig. 6 versus the laser pulse separation $\Delta\tau$. The optimum pulse separation of about 100 ps compares well with the scaling formula of our analytical model. The computed maximum value of the emitted energy corresponds to the efficiency 6.2×10^{-4} of laser energy conversion into the He-α line.

It is deduced from the comparison of energy conversion efficiencies calculated for the conditions of Figs. 5 and 6 that short laser wavelengths are favorable for the x-ray energy in the assumed spectral range due to a higher laser absorption. The estimated maximum peak brilliance is $\simeq10^{21}$ photons/(s mrad^2 mm^2) in 0.1% of the relative bandwidth for laser intensity 5×10^{17} W/cm^2, which is the upper limit of the applicability of our model. Such a brilliance is comparable to the brilliance of the accelerator Bessy II (quoted in Ref. [9]), but it is smaller than the brilliance that can be reached using the optimal foil target [9]. However, using a prepulse is much simpler and high repetition rates are easily achieved. Therefore, it may be interesting for certain applications. To our knowledge, possible further enhancement of line x-ray emission by using both laser prepulse and foil target has not yet been studied and we plan to consider such an option in future.

VI. CONCLUSIONS

A simple method of enhancement of line x-ray emission using subpicosecond laser pulses with a suitable laser prepulse has been studied. A satisfactory agreement of experimental results, analytical scalings, and numerical simulations has been obtained. Our numerical simulations reveal detailed spatial and temporal characteristics of the x-ray line source that may be important for applications.

Our scaling formulas show the dependence of He-α emission on experimental conditions. The emitted energy is maxi-

mal for an optimum pulse separation that increases when the main pulse intensity is decreasing.

A special shape laser pulse (two pulses with the same pulse duration, different intensities, and long pulse separation) is shown to be capable of increasing the intensity of a suitable x-ray line more than ten times. The length of the x-ray pulse may be varied by laser pulse separation. When the energy of the He-α emission is maximal, its pulse duration is $\approx$10 ps.

Experimental implementation of laser double pulses with variable pulse separation is simple and high repetition rates are easily achievable. Thus, using laser double pulses appears to be a viable option for improving the efficiency of an ultrashort-pulse laser-produced line x-ray source.

ACKNOWLEDGMENTS

The support through Research Project J04/98:210000022 of the Ministry of Education of the Czech Republic is gratefully acknowledged. The Grant Agency of the Czech Republic (Contract Nos. 202/97/1186 and 202/01/0755) supported the collaboration of J.L. with A.B.I. The authors want to express their gratitude to Professor L. Kocbach for fruitful, stimulating discussions.

[1] M. Murnane, H. Kapteyn, and R. Falcone, Phys. Rev. Lett. **62**, 155 (1989).
[2] J. C. Kieffer, M. Chaker, J. P. Matte, C. Y. Cote, Y. Beaudoin, Z. M. Jiang, S. Coe, G. A. Mourou, O. Peyrusse, and D. Gilles, Proc. SPIE **1860**, 127 (1993).
[3] U. Teubner, G. Khnle, and F. P. Schfer, Appl. Phys. B: Photophys. Laser Chem. **B54**, 493 (1992).
[4] H. Nakano, T. Nishikawa, H. Ahn, and N. Uesegi, Appl. Phys. Lett. **69**, 2992 (1996).
[5] A. A. Andreev, V. I. Bayanov, A. B. Vankov, A. A. Kozlov, I. V. Kurnin, N. A. Solovyev, S. A. Chizhov, and V. E. Yashin, Quantum Electron. **27**, 76 (1997).
[6] P. Alaterre, C. Chenais-Popovics, P. Audebert, J. P. Geindre, and J. C. Gauthier, Phys. Rev. A **32**, 324 (1985).
[7] J. N. Broughton and R. Fedosejevs, J. Appl. Phys. **74**, 3712 (1993).
[8] D. Altenbernd, U. Teubner, P. Gibbon, E. Förster, P. Audebert, J. P. Geindre, J. C. Gauthier, G. Grillon, and A. Antonetti, J. Phys. B **30**, 3969 (1997).
[9] U. Teubner, U. Wagner, D. Obershmidt, P. Gibbon, E. Foerster, A. Andreev, T. Wilhein, and U. Vogt. *High Brightness X-Radiation and Plasmas Frequency Emission from Femtosecond Laser Plasmas*, edited by E. Foerster, D.D. Meyerhofer, and W. Sander, Application of High Field and Short Wavelength Sources VIII, Technical Digest Series 8 (OSA, Washington, D.C., 1999).
[10] G. A. Mourou, C. P. J. Barty, and M. D. Perry, Phys. Today **51** (1), 22 (1998).
[11] A. A. Andreev, T. Ueda, and J. Limpouch, Proc. SPIE **4343**, 789 (2001).
[12] A. A. Andreev, U. Teubner, I. V. Kurnin, and E. Förster, Appl. Phys. B: Lasers Opt. B **70**, 505 (2000).
[13] H. Nakano, T. Nishikawa, N. Uesugi, J. Limpouch, and A. A. Andreev, Proc. SPIE **4424**, 456 (2001).
[14] H. Nakano, P. Lu, T. Nishikawa, and N. Uesugi, Inst. Phys. Conf. Ser. **159**, 535 (1998).
[15] A. A. Andreev, J. Limpouch, and H. Nakano, Proc. SPIE **3934**, 52 (2000).
[16] A. A. Andreev and J. Limpouch, J. Plasma Phys. **62**, 179 (1999).
[17] K. Eidmann, J. Meyer-ter-Vehn, T. Schlegel, and S. Hüller, Phys. Rev. E **62**, 1202 (2000).
[18] R. W. Lee, B. L. Whitten, and R. E. Stout, J. Quant. Spectrosc. Radiat. Transf. **32**, 91 (1984).
[19] Y. T. Lee, and R. M. More, Phys. Fluids **27**, 1273 (1984).
[20] M. V. Ammosov, N. B. Delone, and V. P. Krainov, Zh. Eksp. Teor. Fiz. **91**, 2008 (1986) [Sov. Phys. JETP **64**, 1191 (1986)].
[21] I. G. Lebo, I. V. Popov, V. B. Rozanov, and V. F. Tishkin, J. Russ. Laser Res. **15**, 136 (1994).
[22] M. Salter, R. W. Lee, and L. A. Jobs, J. Quant. Spectrosc. Radiat. Transf. **39**, 139 (1988).
[23] J. P. Apruzese, J. Davis, D. Duston, and R. W. Clark, Phys. Rev. A **29**, 246 (1984).
[24] D. Riley, J. Quant. Spectrosc. Radiat. Transf. **60**, 221 (1998).
[25] O. Peyrusse, Phys. Fluids B **4**, 2007 (1992).
[26] G. Rybicki, in *Methods in Radiation Transfer*, edited by W. Kalkofen (Cambridge University Press, Cambridge, 1984).
[27] I. I. Sobelman, L. A. Vainstein, and E. A. Yukov, *Excitation of Atoms and Broadening of Spectral Lines* (Springer, Heidelberg, 1995).
[28] M. D. Rosen, Proc. SPIE **1229**, 160 (1991).
[29] D. F. Price, R. M. More, R. S. Walling, G. Guethlein, R. L. Shepherd, R. E. Stewart, and W. E. White, Phys. Rev. Lett. **75**, 252 (1995).
[30] A. A. Andreev, J. Limpouch, and A. N. Semakhin, Izv. Akad. Nauk, Ser. Fiz. **58**, 167 (1994) [Russ. Acad. Sci. Bull. Phys. **58**, 1056 (1994)]; J. Limpouch, A. A. Andreev, and A. N. Semakhin, Proc. SPIE **1980**, 75 (1992).
[31] A. B. Langdon, Phys. Rev. Lett. **44**, 575 (1980).
[32] A. R. Bell, J. R. Davies, and S. M. Guerin, Phys. Rev. E **58**, 2471 (1998).